



SEISMIC ASSESSMENT OF REINFORCED CONCRETE BUILDINGS WITH COUPLED WALLS

L. Ramos ⁽¹⁾, M. A. Hube ⁽²⁾

⁽¹⁾ PhD Student, Pontificia Universidad Católica de Chile, lramos1@uc.cl

⁽²⁾ Associate Professor, Department of Structural and Geotechnical Engineering and National Research Center for Integrated Natural Disaster Management CONICYT/FONDAP/15110017, Pontificia Universidad Católica de Chile, mhube@ing.puc.cl

Abstract

In Chile, most reinforced concrete (RC) buildings have a shear wall configuration, which in a large majority have performed well during recent earthquakes. However, a brittle failure was observed in RC walls in few buildings after 2010, Mw=8.8, Chile earthquake. This flexural-compressive failure was observed in RC walls located at lower stories. Inelastic dynamic analysis conducted recently demonstrated that these buildings remained essentially elastic until an abrupt failure occurred in RC walls. Therefore, investigating the elastic dynamic behavior of such buildings is critical to further understand the seismic behavior and the observed damage. Additionally, recent studies on resisting planes of RC buildings damaged during the Chile earthquake suggest that the behavior of the walls was highly influenced by the interaction of the resisting plane with the rest of the structure. Motivated by these hypotheses, the main objective of this research is to assess the coupling effect in walls considering the three-dimensional layout of RC buildings. The second objective is to analyze the effects of four modeling assumptions in the seismic demand of coupled RC walls. To achieve these objectives, detailed linear finite element models of three RC wall buildings damaged during 2010 earthquake are developed in ETABS and response history analyses are conducted applying ground motions in both horizontal directions simultaneously. From these analyses, the seismic demand of axial loads, shear forces, and bending moments along the height of several RC walls is investigated. Results show that the common design assumption of a cantilever wall implicit in design codes is inappropriate for this type of buildings. From this study it is concluded that the axial load of walls increases considerably due to coupling effect, with values that exceed an axial load ratio of 0.35, which corresponds to the limit imposed after 2010 Chile earthquake.

Keywords: reinforced concrete, walls, coupling behavior, building, axial load



1. Introduction

Reinforced concrete (RC) shear wall buildings are widely used in the world due to its capacity to withstand seismic loads, to control lateral displacements and to limit the damage on nonstructural components. In Chile, residential buildings have a shear wall configuration, typically with a fish-bone plane layout, which in a large majority performed well during the 2010 Chile earthquake [1].

Previous studies on RC shear wall buildings [2-5] concluded that buildings remained essentially elastic during 2010 Chile earthquake, until an abrupt brittle failure occurred in some cases. Other study [6] suggests that the behavior of damaged walls was highly influenced by the interaction of such walls with the rest of the structure, which generated a non-linear distribution of bending moment along the walls height. Therefore, seismic demands in RC walls of such buildings with coupled walls are not properly captured by typical approaches used for building design, such as the one in the ACI 318-14 [7]. In this code, a cantilever behavior is assumed for the seismic design of RC walls. Therefore, the difference between the actual and the assumed behavior suggests that RC wall design assumptions and procedures needs to be revised for Chilean buildings.

Several research efforts have been conducted to assess the behavior of RC coupled walls. These studies have contributed to identify optimal geometrical configurations for coupled walls [8] and its failure mechanism by using real scale models [9]. A pre-design method has also been proposed [10], and a comparison between the force and displacement methods for designing coupled walls has been performed [11]. Finally, fox et al. [12] compared three different methods for capacity design of coupled walls. Despite these efforts, several questions remain unsolved and more research is required regarding the seismic behavior of RC coupled walls.

The objective of this study is to assess the coupling effect in RC walls considering the three-dimensional layout of Chilean fishbone buildings. In particular, the seismic demand of axial load, shear force, and bending moment along wall heights are investigated. Additionally, the effects of using different modeling assumptions on the seismic demand of these walls are investigated.

Three buildings damaged during the 2010 earthquake are used to assess the elastic seismic demand in RC walls. This type of analysis is justified as building remained essentially elastic until a brittle failure occurred [2-5]. Nonlinear models will be analyzed in a future stage of this research. For this study, the buildings are analyzed using detailed finite element models in ETABS [13] and four different modelling assumptions are considered to account for different stiffnesses of beams, walls, and slabs. For the first model a rigid in-plane diaphragm, but with finite bending stiffness is considered, as commonly assumed in engineering practice. For the other three models a semi-rigid diaphragm is considered. For the third and fourth models, reduced stiffnesses are considered in beams, walls and slabs to simulate the cracking behavior of the structural elements. The seismic demand for each building is estimated from response history analyses using four seismic records from 2010 Chile earthquake, and the ground motions are applied considering both horizontal direction simultaneously. From the presented analyses, the height distribution of axial load, shear force, and bending moment is obtained for selected walls in the three buildings.

2. Buildings Descriptions

Three buildings damaged during 2010 Chile earthquake are considered in this study. Two of these buildings are located in Concepción (CM and AH), and one in Santiago (SO). The city of Concepción is located at 105 km SSW from the epicenter and was the most damaged city after the earthquake. Santiago is located at about 450 km north from Concepción.

The selected buildings experienced moderate to severe damaged concentrated mainly in RC walls located at the first basement and the first floor. Table 1 summarizes general characteristics of the considered buildings. The table includes the city, number of stories, built year, floor plan area, and the soil type used for designing the buildings. Soil type II represents a dense gravel or clay with shear wave velocity larger than 400 m/s in the upper 10 m, and soil type III represents a gravel or clay with shear wave velocity lower than 400 m/s [14]. A_o is maximum peak ground acceleration according to NCh433 [14].

Table 1 – RC buildings considered in this investigation

ID	City	# Stories	Built year	Floor plan area (m ²)	Soil type	A _o (g)
CM	Concepción	18+1	2005	13,870	III	0.4
AH	Concepción	15+2	2009	12,665	III	0.4
SO	Santiago	18+2	2007	10,190	II	0.3

The plan views of the typical story for the three considered buildings are shown in Fig. 1, where it is shown that the three buildings have a relatively rectangular plan layout. The CM building in Concepción has 18 stories and 1 basement and it contains commercial spaces in the first level. The structural system comprises RC walls with a typical thickness of 20 cm, 15 cm thickness slabs, and some inverted beams 20 cm wide, and 50 to 150 cm depth. The AH building has 15 stories and 2 basements and the thickness of typical walls is 20 cm. The thickness of the slabs is 15 cm in upper stories and 20 cm in the two basements. The building is also structured with a few beams of 20, 30 and 40 cm width, and depths that range from 35 to 150 cm. Finally, the SO building has 18 stories and 2 basements, and is composed by two symmetrical rectangular blocks separated by a construction joint (Fig. 1c shows one of these blocks). The thickness of the walls is 20 cm, and the thickness of the slabs is 15 cm. The SO buildings also contain few deep beams of dimensions 20 by 75 cm. More information about these buildings is available elsewhere [3-5].

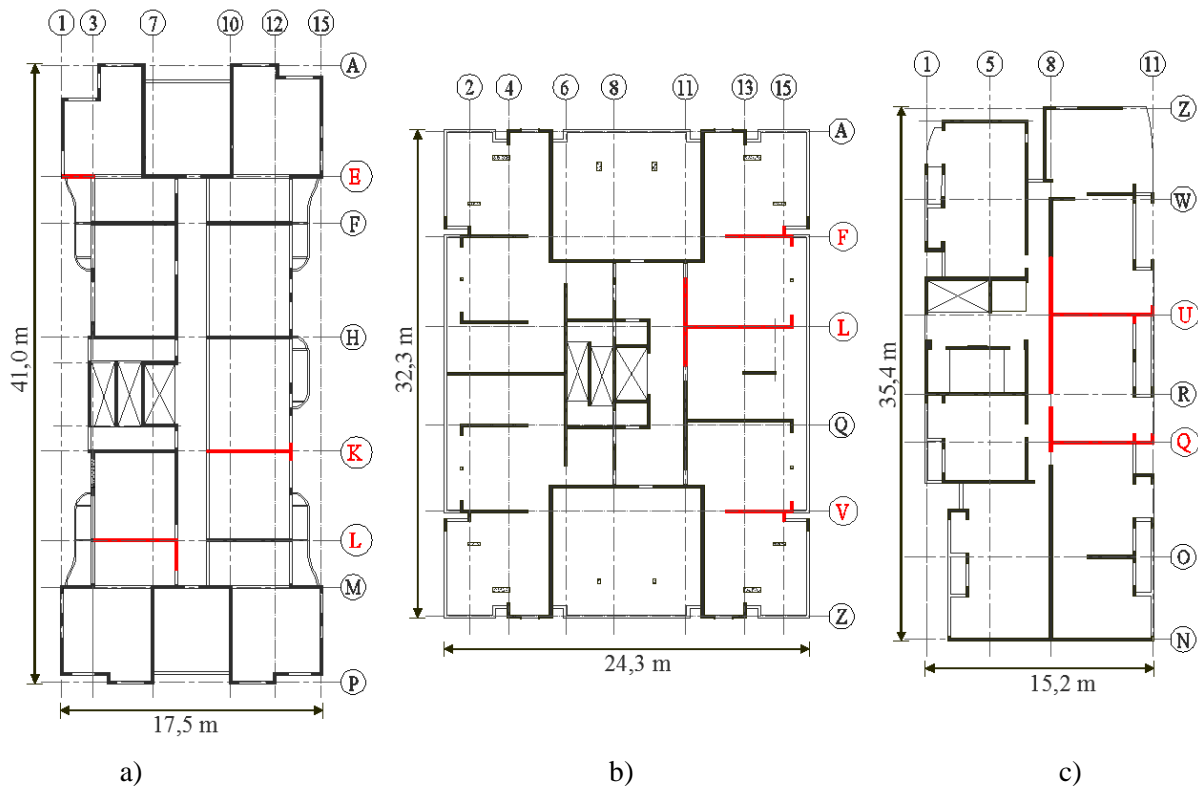


Fig. 1 – Plan view of typical story of considered buildings: a) building CM; b) building AH; c) building SO. Considered walls in this study are shown in red.

3. Finite Elements Models

The elastic seismic response of the described buildings is obtained using finite element models constructed in ETABS [13]. The analytical models of the buildings are shown in Fig. 2. In these models, the walls and slabs are modeled with 4-node shell elements with thin plate formulations. Beams are modeled as frame elements and the soil-structure interaction is not considered. Fixed supports are considered in the base, and the building mass is calculated from the dead load and 25% of the live load.

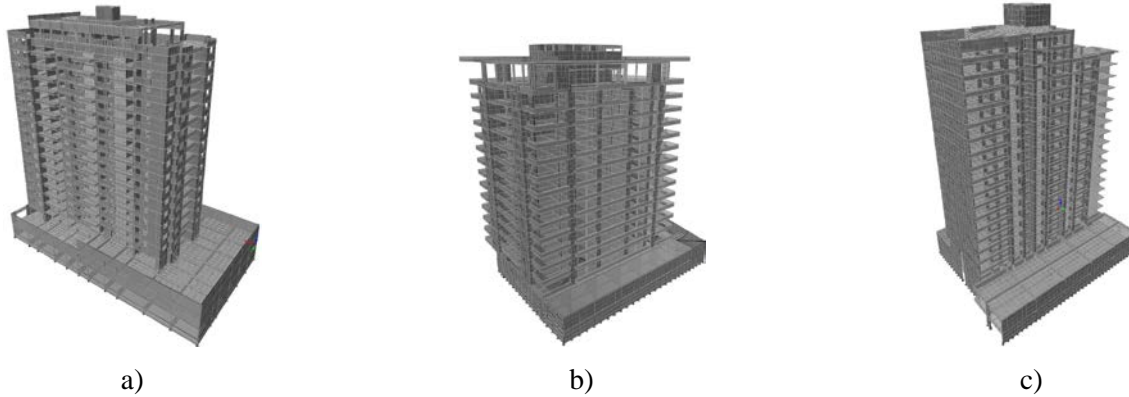


Fig. 2 – 3D views of the finite element buildings: a) CO building; b) AH building; c) SO building

For each building, four different modeling assumptions are considered to assess the effect of the diaphragm flexibility and the effective stiffness of the elements on the elastic seismic response. Table 2 summarizes the four modeling assumptions considered for each building. The first model (R) considers rigid in-plane diaphragm with bending stiffness, and gross moment of inertia for the structural elements, which are common assumptions adopted in engineering practice. The model SR0 is identical to mode R, but considers a semi-rigid diaphragm, which incorporates in-plane stiffness. The last two models consider semi-rigid diaphragms, and the structural elements are modeled with reduced stiffness to consider the cracked stiffness of the elements. For model SR1, the reduced moment of inertia proposed by ACI 318-14 [7] for factored load analysis are considered. Finally, for SR2 model, the same moments of inertia as SR1 model are used for beams, columns and walls, but a larger moment of inertia is considered for slabs to simulated a less cracked slab. Reduced shear stiffness is not considered in walls as they are not prescribed in the ACI 318-14 [7].

Table 2 – Modelling assumptions considered for each building

ID Model	Diaphragm	Moment of Inertia			
		Beams	Columns	Walls	Slabs
R	Rigid	I_g	I_g	I_g	I_g
SR0	Semi-rigid	I_g	I_g	I_g	I_g
SR1	Semi-rigid	$0.35 I_g$	$0.7 I_g$	$0.5 I_g$	$0.25 I_g$
SR2	Semi-rigid	$0.35 I_g$	$0.7 I_g$	$0.5 I_g$	$0.4 I_g$

The fundamental periods of the analyzed buildings with the four modelling assumptions are summarized in Table 3. The periods for the R models are equivalent to those in Westenenk et al. [2], and Jünemann et al. [4]. When the in-plane stiffness of the diaphragm is considered, the periods of SR0 models increase about 3% with respect to those of the R models. These period differences are lower than those observed for free-plan reinforced concrete buildings when modeling the building with rigid or semi-rigid diaphragm [15]. When the reduced moment of inertia is considered, the Table 3 shows that the periods increase about 33% with respect to those of the models SR0, and about 35% with respect to those of the models R.



Table 3 – Estimated fundamental periods of the considered buildings

ID Modelo	T (s)		
	CM	AH	SO
R	0.814	0.603	0.865
SR0	0.834	0.628	0.882
SR1	1.242	0.922	1.332
SR2	1.204	0.892	1.274

3.1 Ground Motions

Ground motions for the response history analyses are selected based on buildings' location from the available records of the 2010 Chile earthquake. Seismic records from San Pedro (SP) [16] and Concepcion (CO) stations [17] are used for buildings located in Concepcion. For the building SO located in Santiago, the seismic records Santiago Centro (SC) and Santiago Peñalolén (SN) [17], are selected. The PGAs of the considered ground motions are shown in Table 4. Both horizontal components of seismic records (NS y EW) are applied simultaneously at the buildings considering the two possible orientations of the ground shaking (i.e aligning the NS component of a ground motion with the longitudinal direction of the buildings, or with the transverse direction of the buildings). The pseudo-acceleration spectrum and displacement spectrum of the two horizontal components of the four ground motions are shown in Fig. 3.

Table 4 – Peak ground accelerations of ground motions and scaling factors for each building

Ground Motion	PGA (g)	Scaling Factors		
		CM	AH	SO
CO_EW	0.29	1.33	2.48	--
CO_NS	0.40	0.74	1.41	--
SP_EW	0.58	6.38	6.76	--
SP_NS	0.61	1.58	1.47	--
SC_EW	0.31	--	--	1.71
SC_NS	0.21	--	--	1.82
SN_EW	0.29	--	--	1.15
SN_NS	0.30	--	--	2.06

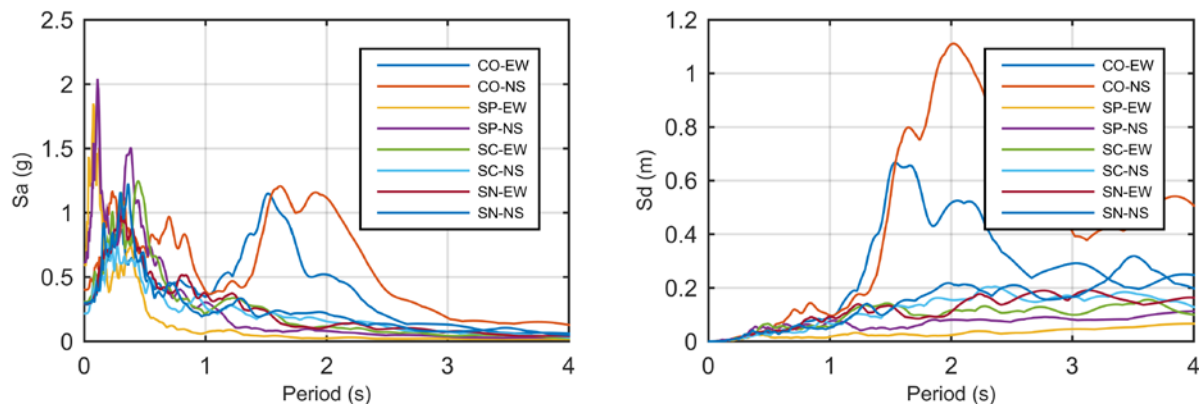


Fig. 3 –Pseudo-acceleration and displacement response spectrum for selected ground motion. 5% critical damping.

For conducting the response history analyses, the seismic records are scaled to a spectral displacement S_d of 10 cm at the fundamental periods of the building obtained with the R model, which on average represents 115% of the design code displacement spectrum at the buildings periods. The design spectrum displacement is obtained using DS61 [18], with the peak ground accelerations and the soil types shown in Table 1. The horizontal component applied in the direction of the damaged walls is considered for obtaining the scaling factor, and the same scaling factor is applied to both horizontal components. The scaling factors considered for each building for the ground motions aligned with the direction of the damaged walls are summarized in Table 4.

4. Results

This section summarizes the seismic demand from the response history analyses of the red walls of the three buildings in Fig. 1. Detailed results are presented for the right side wall of axis K in CM building, and for the right side wall of axis F in AH building. The selected walls have a thickness of 20 cm and a variable cross section along their height, as shown in Fig. 4. Wall in elevation K has an L shape in the basement and first level, which changes to a T-shape in the upper stories of the building. The number of beams connected to this wall, shown in red in the cross sections of Fig. 4, vary along the wall's height, as well as the beams dimensions.

The selected right wall in axis F of building AH is a flag-shape wall. The wall has a rectangular cross section from the second basement to the 1st floor. For the upper stories, the length of the wall is larger, and the cross section contains flanges at the exterior side of the building. The wall has the same cross section from the floor 2 to 13, and the cross section in 14th floor is different. Additionally, the number and cross section of connecting beams varies along the wall's height.

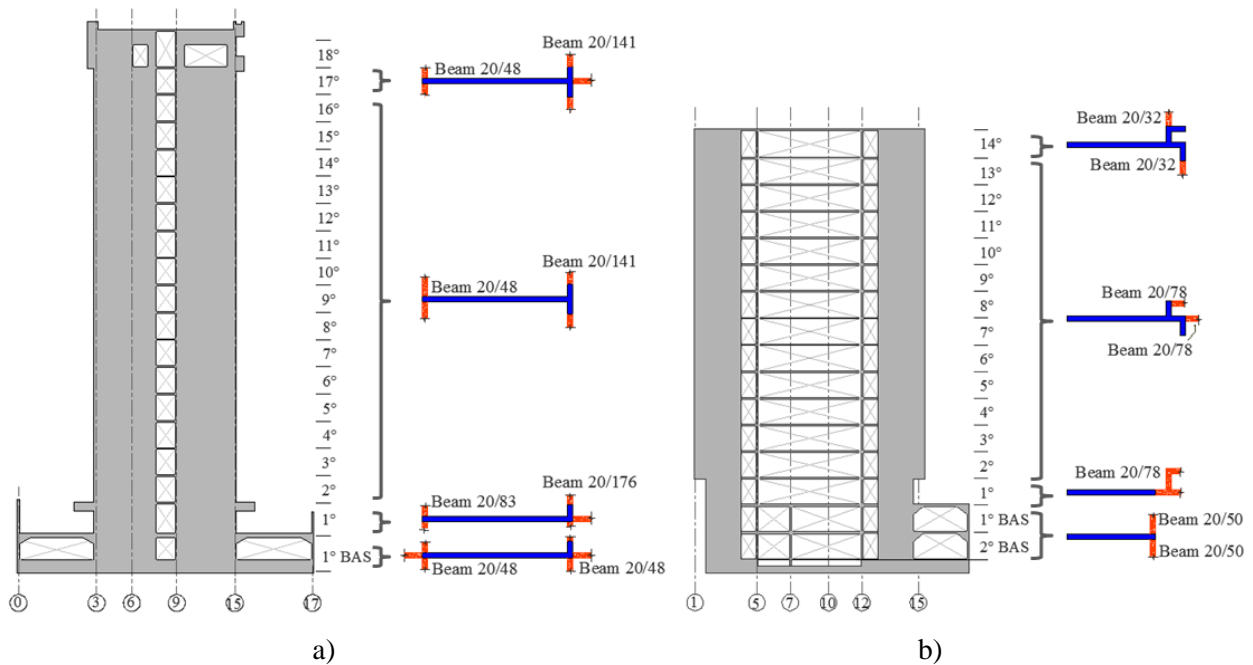


Fig. 4 – Elevation view and cross sections of the selected walls: a) Axis K of CM building; b) Axis F of AH building.

The seismic demand of axial load, shear force, and bending moment for the two walls in Fig. 4 are shown in Fig. 5 and Fig. 6, respectively. The figures show the force distributions at the time of maximum and minimum roof displacement for the scaled CO ground motion, and for the four modeling assumptions (R, SR0, SR1, SR2). The blue lines are the results when the EW component of the ground motion is applied in the direction of the damaged walls in each building, while the NS component is applied in the perpendicular direction. The red lines are the results when the horizontal components of the ground motions are exchanged.

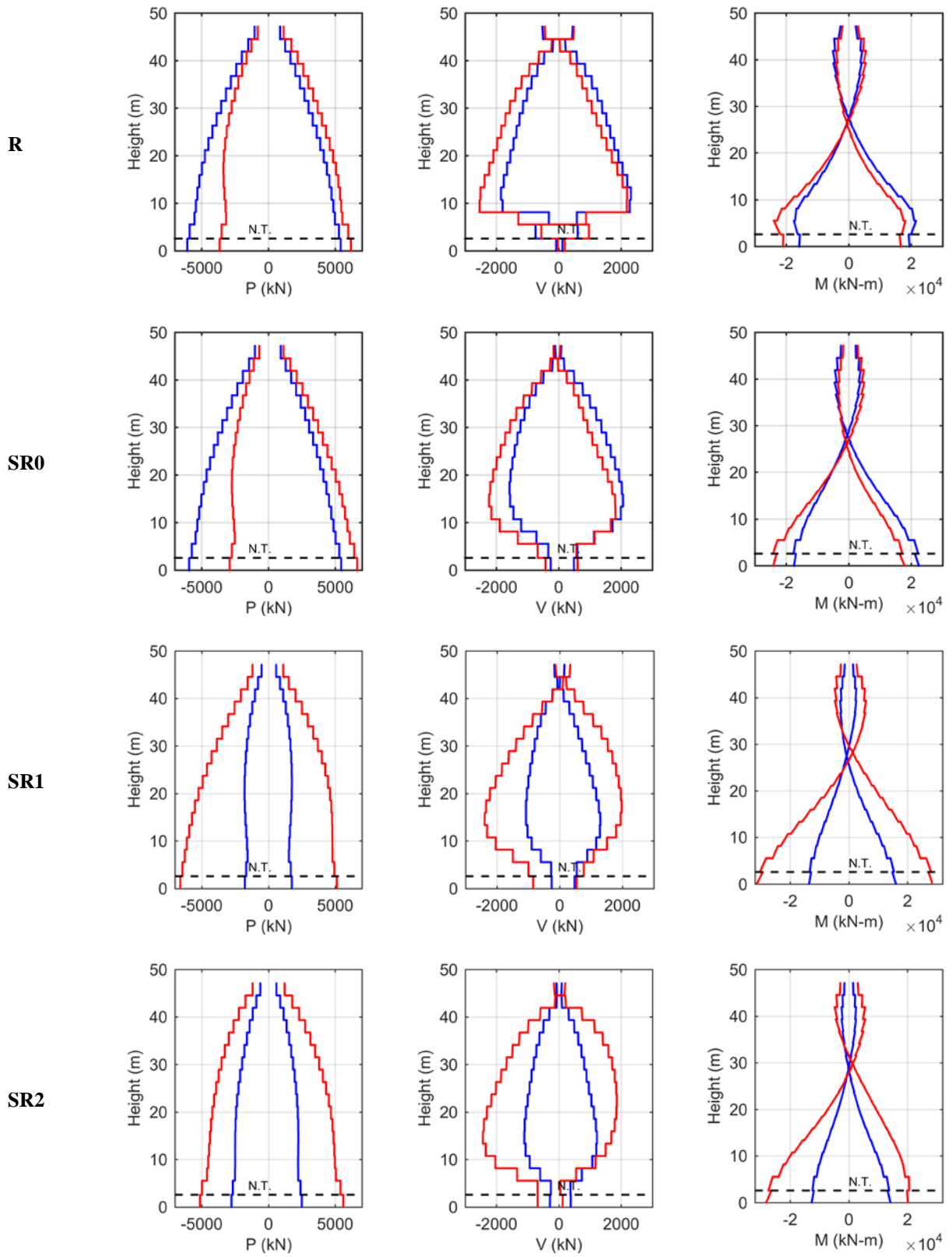


Fig. 5– Seismic demand of axial loads (P), shear (V), and bending moments (M) along the height of the selected wall in axis K of CM building for CO ground motion.

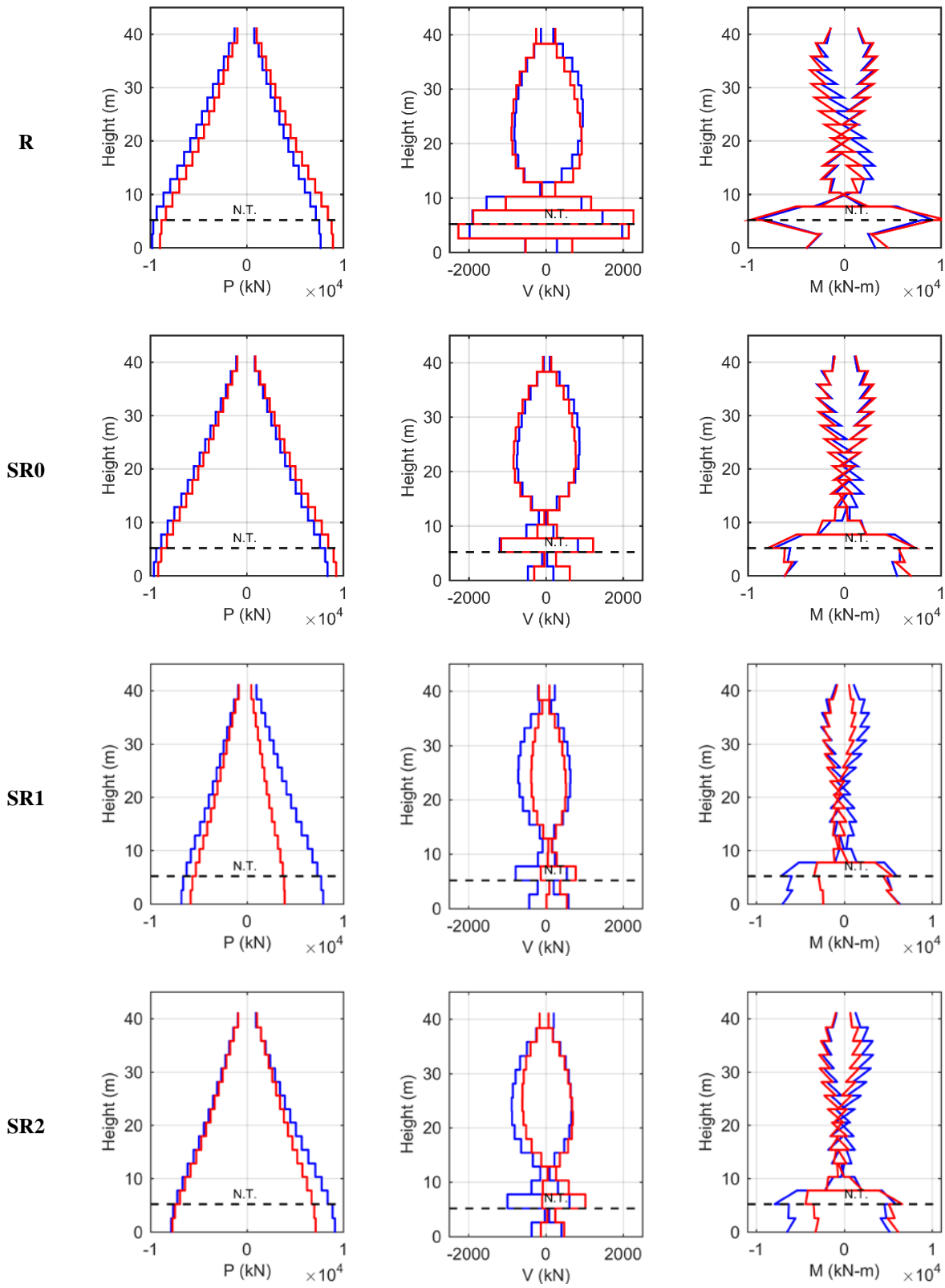


Fig. 6 –Seismic demand of axial loads (P), shear (V), and bending moments (M) along the height of the selected wall in axis F of AH building for CO ground motion.



For the selected wall in axis K of building CM, Fig. 5 shows that the axial load increases considerably in lower stories for the case with modeling assumption R. For this case, the maximum seismic axial load is 6,157 kN in tension and 6,075 kN in compression. These axial loads are equivalent to axial load ratios of 0.20 for both tension and compression. The maximum shear demand of 2,542 kN is observed at the third story. Below this story, the shear decreases considerably and the sign of the shear forces even reverses due to the back-stay effect. From the bending moment diagram, Fig. 5 shows that the wall is deformed with double curvature as the sign of the bending moment changes at about 53% of the building height (story 10). A maximum bending moment of 23,980 kN-m is predicted at top of the first story.

When the diaphragms are assumed semi-rigid (model SR0), the predicted axial loads and bending moments varies slightly, when compared to those of the R model. However, larger differences are observed for the shear forces, where the back-stay effect is not that pronounced in model SR0. For this model, a maximum shear of 2,239 kN is predicted at the 5th story.

For the models with reduced stiffness, Fig. 5 shows that with respect to the R model, the predicted maximum axial load for the SR1 model (6,597 kN) increases by 9%, while for SR2 model (5,591 kN) decreases by 9%. For the SR1 model, and when the EW component of the ground motion is applied in the direction of the damaged walls of the buildings (blue line in Fig. 5), the maximum axial load is not predicted at the base of the wall, but at the 8th story. However, the axial load is relatively constant from the base to such story in this case. Regarding the bending moment, the maximum bending moment in SR1 and SR2 models are respectively 30% and 17% larger than that predicted by the SR0 model.

The axial load demand pattern of the wall in axis F of building CO (Fig. 6) is similar to that observed for the wall in axis K of building AH (Fig. 5), with maximum tension and compression values of 9,825 kN and 8,904 kN for the R model, respectively. These axial loads are equivalent to axial load ratios of 0.58 and 0.53 in tension and compression, respectively. When comparing to the previous wall, larger differences are observed for the shear demand, where reduced values are predicted at two stories for wall in axis F: the second basement and the fourth story. The maximum shear predicted by the R model for wall in axis F is 2,275 kN. Finally, three sign changes are observed in the bending moment diagram for this wall, where the upper change is observed at the same height as that of the K wall (57% of building height).

Finally, when modeling assumption SR1 is considered, the maximum axial load of the wall in axis F of building AH decreases around of 54%, changing from 9,825 kN to 5,853 kN in compression, and from 8,905 kN to 3,891 kN in tension (Fig. 6). Regarding the bending moment, the maximum bending moment in SR1 and SR2 models are respectively 30% and 17% larger than those predicted by the SR0 model.

Based on the presented results of the two walls, it is concluded that the effect of the in-plane stiffness of the diaphragm is negligible in predicting the maximum axial loads. Contrarily, the in-plane stiffness of the diaphragm affects the predicted maximum bending moment. Additionally, for both walls, the bending moment in the second basement is significantly increased when diaphragm is modeled as semi-rigid (Models SR0). Finally, it is concluded that the use of the effective stiffness for structural elements has a significant impact in the predicted axial loads along the wall height, and a reduced impact in the predicted bending moments.

The maximum roof displacement predicted for the analyzed buildings, with the four modelling assumptions, are shown in Table 5. The values show that the mean roof displacement of the four models is 18.9 cm, 1.9 times larger than the considered spectral displacement. The average maximum interstory drift recorded is 0.41%, with a 16 and 84 percentile values of 0.30% and 0.65%. Larger values are predicted in the models with effective stiffness (SR1 and SR2).



Table 5- Maximum roof displacement (cm) predicted for each building.

ID. Building	ID. Model	CO		SP	
		E1	E2	E1	E2
CM	R	15.1	15.3	15.5	16.7
	S0	15.8	15.8	15.2	16.7
	S1	19.7	42.5	11.6	34.6
	S2	19.0	38.7	13.3	33.5
AH	R	14.6	14.2	14.7	14.4
	S0	15.5	16.1	14.2	16.3
	S1	30.3	22.7	13.9	14.3
	S2	30.4	24.7	13.5	14.1
SO		SC		SN	
	R	16.7	17.2	13.6	4.2
	S0	16.9	15.5	14.4	4.4
	S1	28.4	37.4	16.3	8.7
	S2	29.3	37.4	17.8	7.7

Table 6 summarizes the axial load ratios for the selected eight walls of the three buildings. The table includes the cross section area (A_g) at the first story (i.e. critical story for the buildings), and the axial load ratio for dead load, live load, and the predicted maximum seismic axial load ratios for each of the four modeling assumptions. The values shown for the seismic load corresponds to the average axial load ratios predicted by the two ground motions, applied in the two directions. The axial load ratios for dead load varies from 0.07 to 0.19, and the axial load ratios predicted for seismic load varies from 0.08 to 0.57. The results of Table 6 show an average 2% difference between the axial load ratio predicted by the model with rigid diaphragm (R) and the model with semi-rigid diaphragm (SR0). When the effective stiffness of the elements is included in the model, the seismic axial load ratios predicted by the SR1 models is on average 73% lower than those with the SR0 Models. Finally, increasing the slab bending stiffness factor from 0.25 (model SR1) to 0.4 (model SR) increases the axial load ratio by 20% on average. Notably, regardless of the modelling assumption, the axial load ratios that result from the contributions of unfactored dead, live and seismic loads ($D+L+E$) for all walls exceed 0.35, which is the limit imposed after the 2010 Chile Earthquake [13] for ultimate axial loads, with the exception of the Q wall in SO building and the K wall in CM (under SR1 and SR2).

Table 6– Axial load ratios for all selected walls in the three buildings.

Ed.	Axis	A_g (m ²)	D	L	Seismic load (E)			
					R	SR0	SR1	SR2
CM	E	0.44	0.14	0.04	0.51	0.45	0.41	0.48
	K	1.24	0.18	0.05	0.18	0.16	0.11	0.12
	L	1.15	0.12	0.03	0.35	0.38	0.18	0.20
AH	F	0.68	0.18	0.05	0.52	0.54	0.27	0.32
	L	2.36	0.10	0.03	0.38	0.41	0.23	0.25
	V	0.68	0.18	0.05	0.55	0.57	0.28	0.35
SO	Q	3.36	0.07	0.02	0.14	0.14	0.08	0.11
	U	2.14	0.19	0.04	0.27	0.27	0.15	0.19

The wall heights where the maximum shear force and bending moment are predicted for the selected walls of the three buildings, and four modelling cases, are shown in Fig. 7. Purple dots show results for selected walls in the CM building, green dots in AH, and blue dots in SO building. The values are obtained from the shear force and bending moment diagrams at the instant of maximum and minimum roof displacement. The results show that the location of the maximum shear stress at the wall height is not predictable, since it does not follow a clear



trend. Regarding the maximum bending moments, Fig. 7b shows that it occurs mainly at the first 20% of the wall height, and not at the base of the walls, as considered in design codes. Additionally, it is observed that the sign of the bending diagrams of the selected walls of this study changes at least once along the walls height at an average height of 55%.

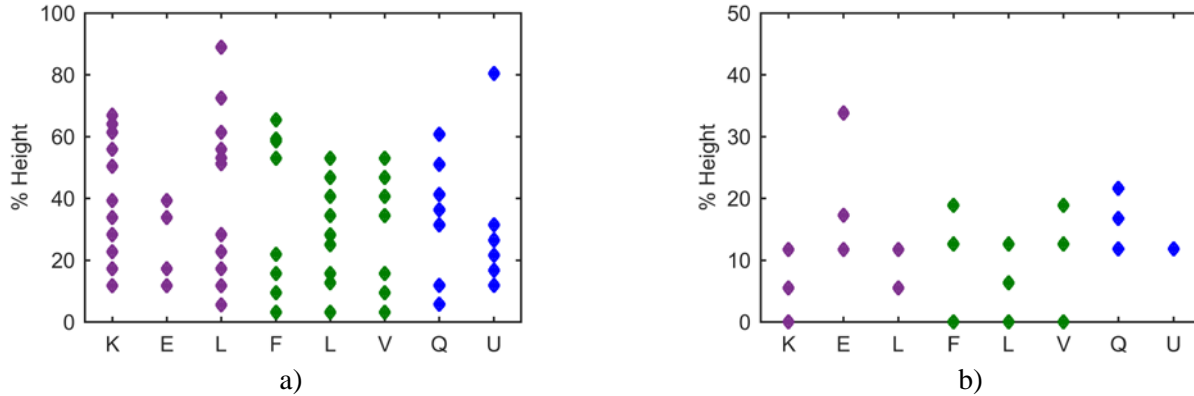


Fig. 7 –Localization of the maximum a) Shear Force. b) Bending moment for eight selected walls

5. Conclusions

Three buildings damaged during the 2010 Maule earthquake are analyzed using elastic finite element models and subjected to ground motion records. Different models are created to evaluate the effect of the stiffness of the diaphragm, walls, beams and slabs on the seismic response of the buildings. The results obtained allows to draw several conclusions about the seismic assessment of elastic RC coupled wall buildings.

For all the walls analyzed in this study, a change in the sign of the bending moment diagram is predicted. This change occurred at about 55% of the building height. Additionally, significant seismic axial loads are predicted at the first story of the walls, which in most cases exceed the axial load ratio limit of 0.35 imposed by the Chilean code after the 2010 Chile Earthquake for ultimate axial loads. These axial loads are generated by the interaction of the walls with the surrounding structural elements. These results are a clear indication that the cantilever assumption of RC walls assumed in ACI-318 is inappropriate for Chilean RC buildings, and the coupling behavior should be considered in design.

Regarding the modeling assumptions, it is concluded that the in-plane diaphragm stiffness has negligible effect on the maximum axial load of the selected walls, but it affects the bending moment diagrams. Changing the diaphragm modelling assumption from rigid to semi-rigid may increase or decrease the maximum bending moments of the walls. Though the buildings sample of this study is small, the results suggest that this phenomenon requires further investigation.

When the buildings are modeled with the effective stiffness factors recommended by ACI-318, an average reduction of the axial load ratios 40% is predicted for the studied walls. The prediction of the axial loads is significantly affected by the effective stiffness of the slab. Therefore, the coupling effect of cracked slabs in RC walls should be investigated in more detail. It is also concluded that the influence of the effective stiffness is smaller for estimating the bending moment than the axial loads in walls.

Finally, it is demonstrated that the stiffness of diaphragms, walls, beams and slabs must be thoughtfully considered for assessing the seismic demands in RC buildings with coupled walls. The coupling effect notoriously influences the axial load, shear, and bending moment demands in Chilean RC buildings.

6. Acknowledgements

This research has been sponsored by the National Research Center for Integrated Natural Disaster Management



CONICYT/FONDAP/15110017. The authors would also like to acknowledge the contribution of Erika Vasquez and Orlando Arroyo. The first author wishes to thank the National Commission for Scientific and Technological Research (CONICYT) for providing her PhD scholarship.

8. References

- [1] Jünemann R, de La Llera JC, Hube MA, Cifuentes LA, Kausel E (2015a): A statistical analysis of reinforced concrete wall buildings damaged during the 2010, Chile earthquake. *Engineering Structures*, **82**, 168-185.
- [2] Wallace JW, Massone LM, Bonelli P, Dragovich J, Lagos R, Lüders C, Moehle J (2012): Damage and implications for seismic design of RC structural wall buildings. *Earthquake Spectra*, **28** (S1), S281-S299
- [3] Westenek B, de la Llera JC, Besa JJ, Jünemann R, Moehle J, Lüders C, Inaudi JA, Elwood K, Hwang SJ (2012): Response of reinforced concrete buildings in Concepción during the Maule earthquake. *Earthquake Spectra*, **28** (S1), S257-S280.
- [4] Westenek B, de la Llera JC, Jünemann R, Hube MA, Besa JJ, Lüders C, Inaudi JA, Riddell R, Jordán R (2013): Analysis and interpretation of the seismic response of RC buildings in Concepción during the February 27, 2010 Chile Earthquake. *Bulletin of Earthquake Engineering*, **11** (1):69–91.
- [5] Jünemann R, de la Llera JC, Hube MA, Vásquez J, Chacón MF (2015b): Study of the damage of reinforced concrete shear walls during the 2010, Chile earthquake. *Earthquake Engineering and Structural Dynamic*, **45**:1621-1641.
- [6] Alarcon C, Hube MA, Jünemann R, de la Llera JC (2015): Characteristics and displacement capacity of reinforced concrete walls in damaged buildings during 2010 Chile earthquake. *Bulletin of Earthquake Engineering*, **13** (4), 1119-1139.
- [7] American Concrete Institute (ACI) (2014): Building code Requirements for Structural Concrete and Commentary, (ACI 318-14), Farmington Hills, MI.
- [8] Harries KA, Moulton JD, Clemson RL (2004): Parametric study of coupled wall behavior-implications for the design of coupling beams. *Journal of Structural Engineering*, **130** (3), 480-488.
- [9] Lehman DE, Turgeon JA, Birely C, Hart CR, Marley KP, Kuchma DA, Lowes N (2013): Seismic behavior of a modern concrete coupled wall. *Journal of Structural Engineering*, **139** (8), 1371-1381 Aksogan et al 2014
- [10] Aksogan O, Turkozer CD, Emsen E, Resatoglu R (2014): Dynamic analysis of non-planar coupled shear walls with stiffening beams using Continuous Connection Method. *Thin-Walled Structures*, **82**, 95-104.
- [11] Fox M, Sullivan T, Beyer K (2014a): Comparison of force-based and displacement-based design approaches for RC coupled walls in New Zealand. *Bulletin of the New Zealand Society for Earthquake Engineering*, **47** (EPFL-ARTICLE-202735), 190-205.
- [12] Fox M, Sullivan T, Beyer K (2014b): Capacity design of coupled RC walls. *Journal of Earthquake Engineering*, **18** (5), 735-758.
- [13] Computers and Structures, Inc. (2010): CSI Analysis Reference Manual for SAP2000, ETABS, SAFE and CSIBridge. Berkeley, California.
- [14] Instituto Nacional de Normalización, INN (1996): Earthquake resistant design of buildings, NCh433 Of.1996. Santiago, Chile (in spanish).
- [15] Chacón MF, de la Llera JC, Hube MA, Marques J, Lemnitzer A (2016): Epistemic uncertainty in the seismic response of RC free-plan buildings. Submitted to *Engineering Structures*.
- [16] Centro sismológico nacional (CSN), Universidad de Chile, Facultad de ciencias Físicas y Matemáticas: <http://www.sismologia.cl/>. Accessed march 2016.
- [17] Universidad de Chile, Departamento de Ingeniería Civil and Oficina Nacional de Emergencia Chile (ONEMI) (2016): Earthquakes of Chile 2010, [http:// terremotos.ing.uchile.cl/2010](http://terremotos.ing.uchile.cl/2010). Accessed march 2016.
- [18] Ministry of Housing and Urbanism, MINVU, DS61, Earthquake resistant design of buildings, replacing D.S. N 117 2010., Diario Oficial, 13 December 2011 [in Spanish].